Origin of volatile element enrichments and alteration of "Rusty Rock" 66095. A new view of volatile element behavior in the lunar crust. C.K. Shearer[1,2], P.V. Burger[1], Z.D. Sharp[2], P.P. Provencio[1], F.M. McCubbin[1,2], A.J. Brearley[2] and A. Steele[3]. [1]Institute of Meteoritics, University of New Mexico, Albuquerque, New Mexico 87131 (cshearer@unm.edu), [2]Department of Earth and Planetary Sciences, University of New Mexico, Albuquerque, New Mexico 87131, [3]Geophysical Laboratory, Carnegie Institution of Washington, Washington D.C. 20015.

Introduction: Apollo sample 66095 consists of a fine-grained, subophitic to ophitic impact melt-rock surrounding a wide variety of lithic clasts [1,2]. Alteration is found in the interior as well as on the surface of "Rusty Rock" 66095. This brownish colored alteration extends from margins of Fe-Ni metal grains into the adjacent silicates and consists of a variety of low-temperature mineral assemblages [1-6]. The origin of this alteration and its associated hydrogen and oxygen isotopic signature have been attributed to alteration on the Moon [7,8], as well as to "terrestrial" alteration during or following transport to Earth [4,9]. Another interesting aspect of 66095 is its enrichment in ^{204}Pb, Cd, Bi, Br, I, Ge, Sb, Tl, Zn, and Cl, indicating that portions of this sample contain a volatile-derived component [10-14]. Similar enrichments have also been observed in Apollo 16 (A-16) soils [8,11-14]. The origin of these enrichments have been attributed to fumarolic-hydrothermal [14], magmatic, or impact processes [11,12]. However, the mineralogical carriers of this volatile-rich component have not been fully identified or characterized [5,8]. This is particularly true of the Cl-bearing mineralogy. Here, we use multiple analytical approaches to examine the alteration mineralogy and geochemistry in 66095 to gain additional insights into its origin and the transport of volatiles in the lunar crust and on the lunar surface.

Analytical approach: We primarily focused our attention on the distribution of Cl and Zn in volatile-bearing mineral phases such as Fe-hydroxides, sulfides, and phosphates. Electron microprobe analyses were conducted on silicates, oxides and sulfides using the JEOL JXA 8200 electron microprobe at the UNM's Department of Earth and Planetary Sciences. Bulk samples of 66095 and Apollo 16 regolith were measured using gas source mass spectrometry at the University of New Mexico with CH_3Cl as an analyte. Details are described in Sharp *et al.* [15]. The alteration mineralogy of 66095 was explored using Raman Spectroscopy following the approaches outlined in [16]. A FEI Quanta 3D Field Emission Gun FIB/SEM/EDS (focused ion beam for extracting site specific areas of the sample, scanning electron microscopy for imaging microtexture, and energy dispersive spectroscopy for identifying Cl- and Zn-rich areas for extraction and conducting chemical analysis), and TEM/STEM/EFTEM (transmission electron microscopy for nano-scale imaging, scanning TEM for chemical contrast, and energy filtered TEM for imaging specific chemical species) were used to examine sub-micron textures, mineralogy, and geochemistry.

Micro-Raman: Micro-Raman imaging indicate akaganéite is the dominant FeO(OH) polymorph, but it is intergrown with goethite. There is some hematite associated with the akaganéite, but it is uncertain whether this phase is a primary alteration phase or a product of alteration during Raman analysis.

EPMA and imaging: Non-leachable Cl phases likely make up the bulk of the Cl-bearing phases observed in thin section. Chlorine in thin sections is closely associated with both FeO(OH,Cl) and phosphates. The FeO(OH,Cl) occurs as rims around metal grains, associated with sulfides, and as dispersed grains in the adjacent matrix. Akaganéites adjacent to these large Fe-Ni metal grains have relatively high concentrations of Ni (1.5-4.4 wt.%) and Co (0.2 to 0.4 wt.%). Nickel and Co concentrations increase toward the Fe-Ni metal interface. Akaganéite is irregularly dispersed in the matrix or associated with sulfides or small Fe-Ni metal grains (<10 μm), and exhibits limited variation in Cl within individual grains. Another interesting aspect of the phosphates assemblage is the identification of stanfieldite, possibly the first in a lunar sample. Previously documented occurrences of stanfieldite have been noted in pallasites and mesosiderites [i.e. 17]. Stanfieldite in 66095 is closely associated with the Fe-Ni-P metal+olivine+plagioclase. Both the olivine and plagioclase have lunar compositions.

Cl isotopes: In the basalts, the δ^{37}Cl ranges from -0.74‰ for coatings on the Apollo 17 orange volcanic glass to +24.5‰ for KREEP basalts. Even higher δ^{37}Cl values have been determined for other KREEP-rich magmatic (i.e. Mg-suite) and lunar impact assemblages. In 66095, the leachate had a Cl isotope composition of +13.95 to +14.08‰. The non-leachable Cl has a composition of +15.59‰. Apollo 16 soils, with volatile element enrichments, have elevated δ^{37}Cl values. The leachate from mature soil (64501) had a Cl isotope composition of +5.6‰ and a non-leachable Cl composition of +15.7‰. The immature soil has a similar Cl isotope composition with the leachate with a Cl isotope composition of +6.1‰ and the non-leachable Cl composition of +14.3‰.

Nano-scale alteration mineralogy: The low-temperature alteration occurs as rims around Fe-Ni metal and sulfide grains, and as dispersed grains in the

adjacent matrix. Transmission electron microscope (TEM) imaging confirms the previous XRD [6] and our micro-Raman data that indicates that akaganéite (βFeO(OH,Cl)) is the dominant FeO(OH) polymorph (Fig. 1). In addition to akaganéite, we have identified goethite, hematite, and feroxyhyte ($\delta Fe^{3+}O(OH)$) using electron diffraction. The identification of hematite and goethite is consistent with micro-Raman observations. These two phases have a distinctly different morphology from the akaganéite. Lawrencite was identified adjacent to Fe-Ni metal using EDS and electron diffraction analysis (Fig. 1). The ring pattern in the electron diffraction pattern indicates that the lawrencite is nanocrystalline. The energy dispersive spectra show some O incorporated into the lawrencite. The lawrencite adjacent to the Fe-Ni alloy reaches a thickness of up to 1µm. TEM observations of the alteration indicate a well-defined "nanometer-scale stratigraphy:" kamacite (body-centered cubic)→face-centered cubic (fcc) Fe-Ni alloy→lawrencite→akaganéite. Alteration adjacent to sulfides exhibits a similar stratigraphy, from sulfides (troilite, sphalerite, griegite)→lawrencite→akaganéite. The lunar lawrencite in 66095 does not react directly to akaganéite. Rather, lawrencite exposed to New Mexico terrestrial conditions reacts to form an amorphous Fe- and Cl-bearing phase, nano-crystalline goethite, and hematite. The morphology of these terrestrial alteration products is significantly different than that of the akaganéite. After extensive study of individual fragments prepared without water, no other alkali or transition metal chlorides (i.e. NaCl, KCl, $MgCl_2$, $ZnCl_2$, $PbCl_2$) were identified in 66095. The apparent absence of these chloride phases may simply reflect the fact that they are present in very low abundances and are distributed heterogeneously within the sample. Alternatively, the conditions of lunar fumarolic activity (gas composition and temperature) may have been outside the stability field for these chlorides. For example, these conditions may have favored the formation of Zn and Pb sulfides rather than chlorides. Textural evidence indicates Zn sulfide-bearing gas reacted with primary troilite to produce sphalerite.

Conclusions: Based on these data it appears likely that the volatile element enrichments and the Cl isotopic fractionation observed in 66095 and the Apollo 16 soils did not result from extra-lunar additions, but are most likely a product of fumarole degassing of a shallow basaltic intrusion or an ejecta blanket. Lawrencite was deposited on mineral surfaces at approximately 650°C to 570°C from a metal-chloride-bearing, H-poor gas phase. This gas phase was also responsible for the transport of other metals (e.g. Zn, Cu, Pb, Fe) and perhaps the fractionation of Cl isotopes. The fractionation of Cl isotopes in the rusty rock can be attributed to fumarole processes in a low-H system or a system evolving from low-H to high-H. The origin and formation of the akaganéite is more enigmatic. The Cl-isotopes are consistent with akaganéite replacing lawrencite. However, numerous nanometer-scale observations are not consistent with a terrestrial origin and indicate multiple episodes of oxyhydration.

References: [1]Garrison, J.R. and Taylor, L.A. (1980) In Proc. Conf. Lunar Highland Crust (ed. Papike and Merrill). 395-417. GCA Supp. 12, Lunar Planetary Institute, Houston. [2]Hunter, R.H. and Taylor, L.A. (1981a) Proc. 12th LPSC 253-259. [3]Hunter, R.H. and Taylor, L.A. (1981b) Proc. 12th LPSC 261-280. [4]Taylor, L.A. et al. (1974) Geology 2, 429-432. [5]El Goresy, A. et al. (1973) Proc. 4th LSC 733-750. [6]Taylor, L.A. et al. (1973) Proc. 4th LSC 829-839. [7]Freidman, I. et al. (1974) Science 185, 346-349.[8] Lunar Sample Compendium. http://curator.jsc.nasa .gov/ lunar/lsc/66095.pdf. [9]Epstein, S. and Taylor, H.P. (1974) Proc. 5th Lunar Sci. Conf. 1839-1854. [10]Nunes, P.D. and Tatsumoto, M. (1973) Science 182, 916-920. [11]Allen, R.O. et al. (1973) Proc. 6th LSC 2271-2279. [12]Hughes, T.C. et al. (1973) Lunar Sci. IV 400-402. [13]Jovanovic, S. and Reed, G.W. (1981) Proc. 12th LPSC 2271-2279. [14]Krahenbuhl, U. et al. (1973) Proc. 4th LSC 1325-1348. [15]Sharp, Z.D. et al. (2010) Science 329, 1050-1053. [16] Steele et al. (2010)Science 329, 51 [17]Davis, A. M. and Olsen, J.E. (1991) Nature 353, 637- 640.

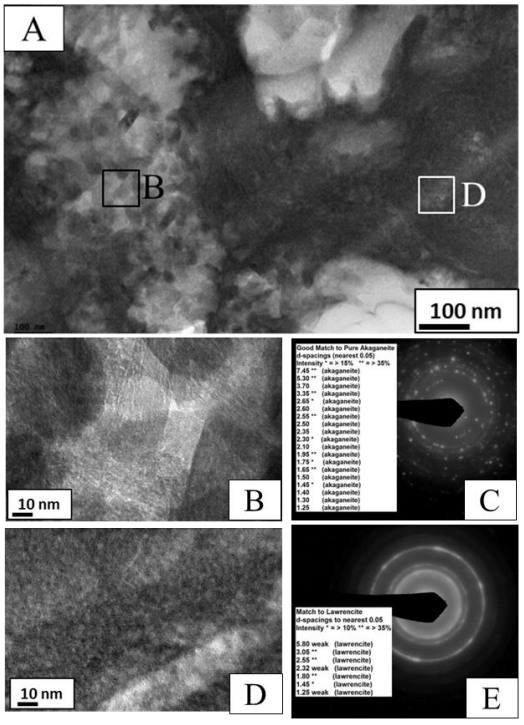

Figure 1. A. Bright-field TEM image of the alteration stratigraphy from body-centered cubic Fe-Ni- alloy (kamacite)→ lawrencite→ akaganéite. B. Bright-field TEM image of akaganéite indexed to location in main image. C. Electron diffraction pattern of phase in Figure 1B. The d spacings identified in the pattern correspond to akaganéite; d spacings are listed in angstroms rounded to the nearest 0.05. D. Bright field TEM image of lawrencite indexed to location in main image. E. Electron diffraction pattern of phase in image Figure 6D. The d spacings identified in the pattern is consistent with lawrencite; d spacings in angstroms. In addition to lawrencite, body-centered cubic Fe-Ni- alloy and hematite were identified in other electron diffraction patterns.